

Dynamic Analysis, Electronic Circuit Realization of Mathieu-Duffing Oscillator and Its Synchronization with Unknown Parameters and External Disturbances

Victor Kamdoum Tamba, François Kapche Tagne,
Elie Bertrand Megam Ngounkadi and Hilaire Bertrand Fotsin

Abstract This chapter deals with dynamic analysis, electronic circuit realization and adaptive function projective synchronization (AFPS) of two identical coupled Mathieu-Duffing oscillators with unknown parameters and external disturbances. The dynamics of the Mathieu-Duffing oscillator is investigated with the help of some classical nonlinear analysis techniques such as bifurcation diagrams, Lyapunov exponent plots, phase portraits as well as frequency spectrum. It is found that the oscillator experiences very rich and striking behaviors including periodicity, quasi-periodicity and chaos. An appropriate electronic circuit capable to mimic the dynamics of the Mathieu-Duffing oscillator is designed. The correspondences are established between the parameters of the system model and electronic components of the proposed circuit. A good agreement is obtained between the experimental measurements and numerical results. Furthermore, based on Lyapunov stability theory, adaptive controllers and sufficient parameter updating laws are designed to achieve the function projective synchronization between two identical drive-response structures of Mathieu-Duffing oscillators. The external disturbances are taken into account in the drive and response systems in order to verify the robustness of the proposed strategy. Analytical calculations and numerical simulations are performed to show the effectiveness and feasibility of the method.

Keywords Dynamic analysis · Mathieu-Duffing oscillator
Electronic circuit realization · Synchronization · Parameter identification
External disturbances

V. K. Tamba (✉) · F. K. Tagne
Department of Telecommunication and Network Engineering, IUT-Fotso
Victor of Bandjoun, University of Dschang, P. O. Box: 134, Bandjoun, Cameroon
e-mail: vkamdoum@gmail.com

V. K. Tamba · E. B. M. Ngounkadi · H. B. Fotsin
Laboratory of Electronics and Signal Processing (LETS), Department of Physics,
Faculty of Science, University of Dschang, P. O. Box: 67, Dschang, Cameroon

1 Introduction

Several problems in physics, chemistry, biology, electronics, neurology and many other disciplines are related to nonlinear self-excited oscillators (Rajasekar et al. 1992). Examples include, the self-excited oscillations in bridges and airplane wings, the beating of a heart and the nonlinear model of a machine tool chatter, the vortex-or flow-induced oscillations in the cylinder of square cross-section and the galloping of transmission lines (Moon and Johnson 1998; Corless and Parkison, 1988, 1993; Yu et al. 1992, 1993a, b). Self-excited oscillators (e.g. Van der Pol, damped Duffing, Duffing-Van der Pol and Duffing-Rayleigh) have been intensively studied and demonstrated to exhibit complex and rich dynamical behaviors including harmonic, subharmonic and superharmonic frequency entrainment (Hayashi 1964), devil's staircase in the behavior of the winding number (Parlitz and Lauterborn 1987) and chaotic behavior with period-doubling cascades (Hayashi 1964; Parlitz and Lauterborn 1987; Guckenheimer and Holmes 1984; Steeb and Kunick 1987). A two-well Duffing oscillator with nonlinear damping term proportional to the power of velocity has been investigated in Anjali et al. (2012). The authors focused their attention on how the damping exponent affects the global dynamical behavior of the oscillator. Analytically, the threshold condition for the occurrence of homoclinic bifurcation using Melnikov technique is derived. The results were supported by numerical simulations. In Venkatesan and Lakshmanan (1997) the authors have demonstrated that a driven Duffing-van der Pol oscillator with a double well potential exhibits rich and striking bifurcation structures such as period-doubling phenomena, intermittencies, crises, transient chaos, and quasi-periodicity. Siewe Siewe and colleagues (Siewe Siewe et al. 2010) have investigated the dynamics of a Duffing-Rayleigh oscillator under harmonic external excitation. They used the Melnikov technique to derive the necessary conditions for chaotic motion of this deterministic system. The effect of damping parameter on phase portraits and Poincaré maps, in addition to the numerical simulations of bifurcation diagram and maximum Lyapunov exponents have been also examined. In Shen et al. (2008), the bifurcation and route to chaos of the Mathieu-Duffing oscillator have been reported using the incremental harmonic balance (IHB) procedure. The authors proposed a new scheme for selecting the initial conditions used for predicting the higher order periodic solutions. The phase portraits and bifurcation points obtained from the IHB method and numerical time-integration were compared yielding a very good agreement. Shen and Chen (2009) investigated the control of chaos in Mathieu-Duffing oscillator using open-plus-closed-loop (OPCL) method. A controller composed of an external excitation and a linear feedback has been designed to entrain chaotic trajectories of Mathieu-Duffing oscillator to its periodic and higher periodic orbits. The critical feedback coefficients under which the chaotic Mathieu-Duffing oscillator is globally and locally OPCL controllable respectively are obtained theoretically and demonstrated numerically. Many other interesting works (Yang et al. 2015; Wen et al. 2016, 2017) have been reported on the fractional-order form of the Mathieu-Duffing oscillator. The authors of these

references studied the effects of the fractional-order on the dynamical behaviors of the integer-order Mathieu-Duffing oscillator. Numerical simulations are performed in their works to validate the theoretical investigations. Motivated by complex dynamical behaviors of self-excited oscillators and their potential applications in many fields, in this chapter, we investigate numerically and experimentally the dynamics and synchronization of a Mathieu-Duffing oscillator in presence of unknown parameters and external disturbances.

Since the idea of synchronization of chaotic systems was introduced by Pecora and Carroll in 1990 (Pecora and Carrol 1990), chaos synchronization has received an increasing attention due to its theoretical challenge and its potential applications in secure communications, chemical reactions, biological systems, information science, and plasma technologies (Zhan et al. 2003). Up to now, many types of synchronization phenomena have been reported. These include complete synchronization (Vincent et al. 2008), phase synchronization (Chitra and Kuriakose 2008), lag synchronization (Zhu and Wu 2004), anticipating synchronization (Zhu and Wu 2004), projective synchronization (Yang et al. 2010), modified projective synchronization (Zhu and Zhang 2009), function projective synchronization (FPS) (Li and Chen 2007), etc. In projective synchronization, the drive and the response systems synchronize up to a scaling factor whereas in modified projective synchronization, the response of the synchronized dynamical state variables synchronizes up to a constant matrix (Kareem et al. 2012). Recently, a more general form of projective synchronization called function projective synchronization (An and Chen 2009; Ping and Yu-Xia 2010) in which drive and response systems are synchronized up to a desired scaling function has attracted much attention of scientists and engineers as it provides more security in its applications to secure communication because the unpredictability of the scaling function matrix. Also, FPS of discrete chaotic systems has now been widely investigated for its great practical application (Fei et al. 2013). Therefore, the research on FPS is more valuable in practice. The majority of the mentioned works are carried out by using the known (certain) parameters of drive and response systems, and the controller is constructed from those known parameters. However, some system's parameters may not be exactly known in advance. In real physical systems, or experimental situations, chaotic systems may have some uncertain or time varying parameters (Mahmoud and Mansour 2011). Moreover, the influence of the uncertainties has been taken into account rarely. It is known that in the real world applications (e.g. secure communication), the systems are affected by various uncertainties including parameter perturbations and external disturbances, which can influence the accuracy of the communication. To our understanding, function projective synchronization of Mathieu-Duffing oscillators with the consideration of unknown parameters and external disturbances has not been explored. The objectives of this chapter are threefold: (a) to consider the dynamics of the Mathieu-Duffing oscillator and investigate its bifurcation structures with particular emphasis on the effects of the amplitude of the parametric excitation; (b) to carry out an experimental study of the dynamics of the system in order to validate the theoretical and numerical results;

and (c) to investigate the synchronization of such a coupled oscillators with unknown parameters and subjected to the external disturbances.

The layout of chapter is as follows. Section 2 deals with the analytical and numerical analysis of the system under study. Some basic properties and bifurcation structures of the system are investigated. The experimental study is carried out in Sect. 3. The laboratory experimental measurements show a qualitative agreement with numerical results. Section 4 deals with FPS between two identical Mathieu-Duffing oscillators in presence of unknown parameters and external disturbances. Numerical simulations are performed in order to illustrate and verify the effectiveness, feasibility and the robustness of the synchronization scheme. Finally, we summarize our results and draw the conclusions of this chapter in Sect. 5.

2 Theoretical Analysis of Mathieu-Duffing Oscillator

2.1 Description of the Model

In this chapter, we consider the Mathieu-Duffing oscillator (Shen et al. 2008) which is described by the following equation of motion:

$$\ddot{x} + 2\varepsilon\dot{x} - (\alpha + \beta \sin \omega t)x + \gamma x^3 = 0 \quad (1)$$

in which $\dot{x} = dx/dt$ represents the derivative with respect to time, ε is the damping coefficient, β and ω are respectively, the amplitude and the frequency of the parametric excitation, α and γ represent respectively, the linear and nonlinear stiffness coefficients. Many mechanical and engineering problems can be really described by Eq. (1). Indeed, it has been used to model the one-mode transverse vibration of the axially moving beam with harmonic fluctuated speed (Shen et al. 2008). The second-order differential Eq. (1) can be transformed into a set of first-order differential equations as follows:

$$\begin{cases} \dot{x} = y \\ \dot{y} = -2\varepsilon y + \alpha x - \gamma x^3 + \beta x \sin \omega t \end{cases} \quad (2)$$

System (2) involves five independent parameters. Due to the relatively large number of parameters, the detailed influence of each parameter on dynamics of the system (2) will be not presented here. The bifurcation structure will be carried out with respect to the amplitude of the parametric excitation because this parameter can be easily varied in the practical situation using a low frequency generator. For the numerical analysis, the following values of parameters will be employed: $\varepsilon = 0.125$, $\alpha = \gamma = 1$, $\omega = 2$ and β variable.

2.2 Dissipativity and Symmetry

To generate chaotic signal, it is necessary for the system to be dissipative. The divergence of system (2) in absence of the external force is evaluated as

$$\nabla V = \frac{\partial \dot{x}}{\partial x} + \frac{\partial \dot{y}}{\partial y} = -2\varepsilon \quad (3)$$

System (2) is dissipative since $\nabla V < 0$. This implies that any volume element $V_0 = V(t=0)$ will be continuously contracted by the flow (i.e. each volume element containing the trajectory shrinks to zero as time evolves to infinity). Then, all system orbits will be confined to a specific bounded subset of zero volume in state space and the asymptotic dynamics settles onto an attractor. The symmetry is one of the interesting characteristics of the dynamical system. This property commonly exists in many nonlinear systems. It is easy to check in absence of external force that system (2) has a natural symmetry since the transformation $S: (x, y) \leftrightarrow (-x, -y)$ is invariant for a specific set of the system parameters. The solution of system (2) that is invariant under the above transformation is called a symmetry solution; otherwise it is called an asymmetry solution.

2.3 Fixed Points Analysis

In absence of external force and by setting the right hand side of system (2) to zero, it is found that there are three equilibrium points $E_1(0, 0)$ and $E_{2,3}(\pm\sqrt{\alpha/\gamma}, 0)$. The characteristic equation obtained at any equilibrium point $E(\bar{x}, \bar{y})$ is defined as

$$\lambda^2 + 2\varepsilon\lambda - (\alpha - 3\gamma\bar{x}) = 0 \quad (4)$$

The characteristic equation for the equilibrium point $E_1(0, 0)$ is

$$\lambda^2 + 2\varepsilon\lambda - \alpha = 0 \quad (5)$$

It is obvious that $E_1(0, 0)$ is always unstable provided that the corresponding characteristic Eq. (5) has coefficients with different signs. For the analysis of stability of the equilibrium points $E_{2,3}(\pm\sqrt{\alpha/\gamma}, 0)$, one only needs to consider since the system is invariant under the transformation $(x, y) \leftrightarrow (-x, -y)$ as mentioned above. Thus, the characteristic equation associated to one of them is defined as follows

$$\lambda^2 + 2\varepsilon\lambda + 2\alpha = 0 \quad (6)$$

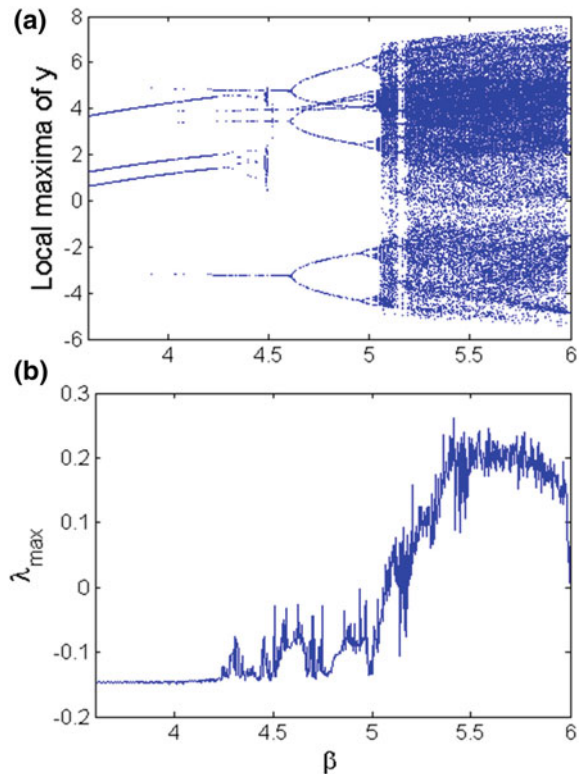
Since ε and α are positive, the equilibrium points $E_{2,3}(\pm\sqrt{\alpha/\gamma}, 0)$ are stable.

2.4 Bifurcation and Chaos

In the numerical results that follow, we investigate the dependence of the system behavior at given angular frequency, linear and nonlinear stiffness coefficients by varying the amplitude of the parametric excitation. The bifurcation diagram shows the projection of the attractors in the Poincaré section onto one of the system coordinates with respect to the chosen control parameter. In order to gain further insight about the dynamics of the oscillator under investigation, we compute the frequency spectrum as well as the largest Lyapunov exponent with the help of the algorithm proposed by Wolf et al. (1985). These results are obtained by solving system (2) with aid of the standard fourth-order Runge Kutta algorithm (Press et al. 1992). The system is integrated for sufficiently long time and the transient is cancelled. The bifurcation diagram showing the local maxima of the coordinate y and the corresponding graph of the largest Lyapunov exponent in terms of the control parameter β varying in the range $3.6 \leq \beta \leq 6$ are provided in Fig. 1 for $\varepsilon = 0.125$, $\alpha = \gamma = 1$ and $\omega = 2$.

In light of Fig. 1a, the extreme sensitivity of the oscillator with respect to small parameter changes is clearly observed. Some interesting dynamical behaviors such

Fig. 1 Bifurcation diagram **a** showing the local maxima of the coordinate y and the corresponding graph of the largest Lyapunov exponent **b** in terms of the control parameter β for $\varepsilon = 0.125$, $\alpha = \gamma = 1$ and $\omega = 2$



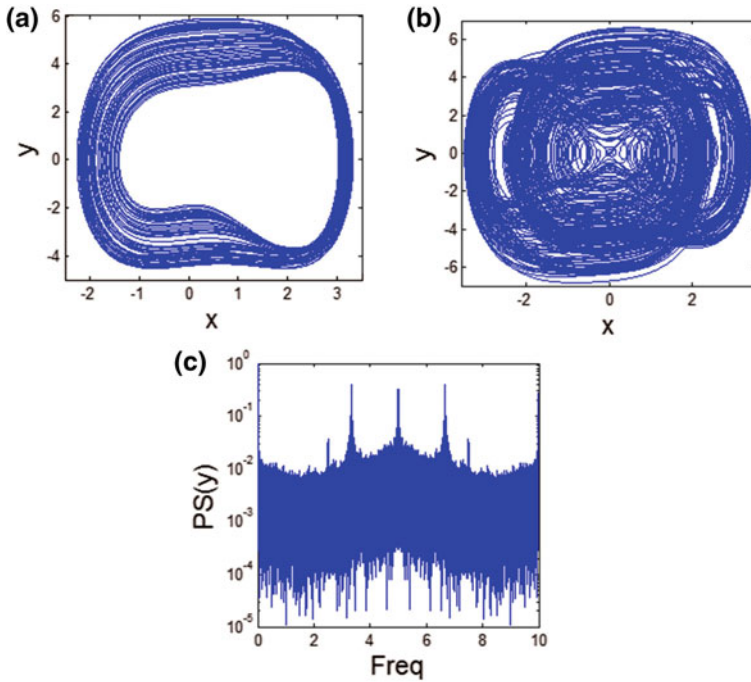


Fig. 2 Chaotic phase portraits of Mathieu-Duffing oscillator computed for $\epsilon=0.125$, $\alpha=\gamma=1$ and $\omega=2$. **a** Single band chaotic attractor for $\beta=5.2$, **b** double band chaotic attractor and **c** frequency spectrum of coordinate y for $\beta=5.8$

as periodicity, quasi-periodicity and chaos are visible. The bifurcation structure is perfectly traced by the largest Lyapunov exponent. Accordingly, some phase portraits showing chaotic states with corresponding frequency spectrum of the system are depicted in Fig. 2.

Asymmetric chaotic attractor is observed in Fig. 2a while a double band strange attractor is depicted in Fig. 2b. The broadband noise-like of frequency spectrum (see Fig. 2c) is signature of the chaotic steady state.

3 Electronic Circuit Realization of Mathieu-Duffing Oscillator

Implementing the theoretical chaotic models using electronic circuits is of great importance for various engineering applications such as robotics, chaos based communications, image encryption and random number generation (Banerjee 2010; Volos et al. 2012, 2013a, b). Moreover, the electronic circuit realization of theoretical chaotic models is an effective approach to investigate the dynamics of such

systems via for instance the experimental bifurcation diagram obtained by varying the values of variable resistors associated to the control bifurcation parameters (Ma et al. 2014; Buscarino et al. 2009). The dynamics of the system under scrutiny has been investigated in preceding paragraphs using theoretical and numerical methods. It is predicted that the system can exhibit very rich and complex behaviors. In this section, in order to validate the numerical results, we design and implement an electronic circuit capable to mimic the dynamical behaviors of system (2). The schematic diagram of the proposed electronic circuit is depicted in Fig. 3.

The electronic circuit of Fig. 3 consists of some analog multipliers used to implement the cubic nonlinear term of the model. They operate over a dynamic range of ± 1 V with typical tolerance less than 1%. The output signal (W) is connected to those at inputs ($+X_1$), ($-X_2$), ($+Y_1$), ($-Y_2$), and ($+Z$) by the following expression $W = (X_1 - X_2)(Y_1 - Y_2)/10 + Z$. The operational amplifiers accompanied with resistors and capacitors are exploited to implement the basic operations such as addition, subtraction and integration. The bias is provided by a 15Volts DC symmetry source. Using the Kirchoff's laws into the circuit of Fig. 3, we obtain its mathematical model given by two coupled first-order nonlinear differential equations

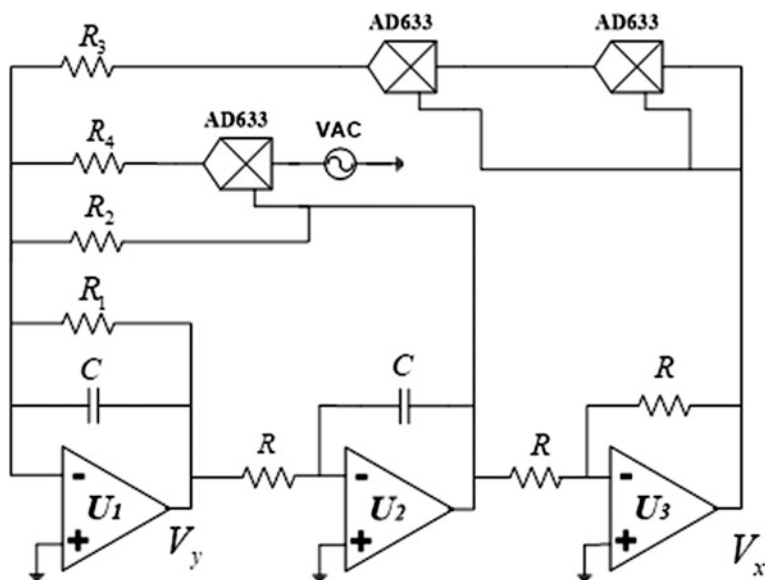


Fig. 3 Electronic circuit realization of the Mathieu-Duffing oscillator. The value of electronic components are fixed as $C = 10$ nF, $R = 10$ k Ω , $R_1 = 40$ k Ω , $R_2 = 100$ Ω , $R_3 = 100$ Ω and R_4 variable. The analog multipliers devices are AD633JN-type while operational amplifiers (U_1, U_2 and U_3) are TL084CN-type ones

$$\begin{cases} \frac{dV_x}{dt} = \frac{V_y}{RC} \\ \frac{dV_y}{dt} = -\frac{V_y}{R_1C} + \frac{V_x}{R_2C} - \frac{V_x^3}{10k_mR_3C} + \frac{V_x \sin \omega t}{k_mR_4C} \end{cases} \quad (7)$$

where V_x and V_y are the output voltages of the operational amplifiers and $k_m = 10$ is a constant introduced by the analog multiplier. The values of components of electronic circuit in Fig. 3 are chosen in order to match system (2) and according to the following change of state variables and parameters: $t = \tau RC$; $x = V_x/1\text{ V}$; $y = V_y/1\text{ V}$; $2\varepsilon = R/R_1$; $\alpha = R/R_2$; $\gamma = R/10k_mR_3$; $\beta = R/k_mR_4$ as follows: $C = 10\text{ nF}$, $R = 10\text{ k}\Omega$, $R_1 = 40\text{ k}\Omega$, $R_2 = 10\text{ k}\Omega$, $R_3 = 100\ \Omega$ and R_4 variable.

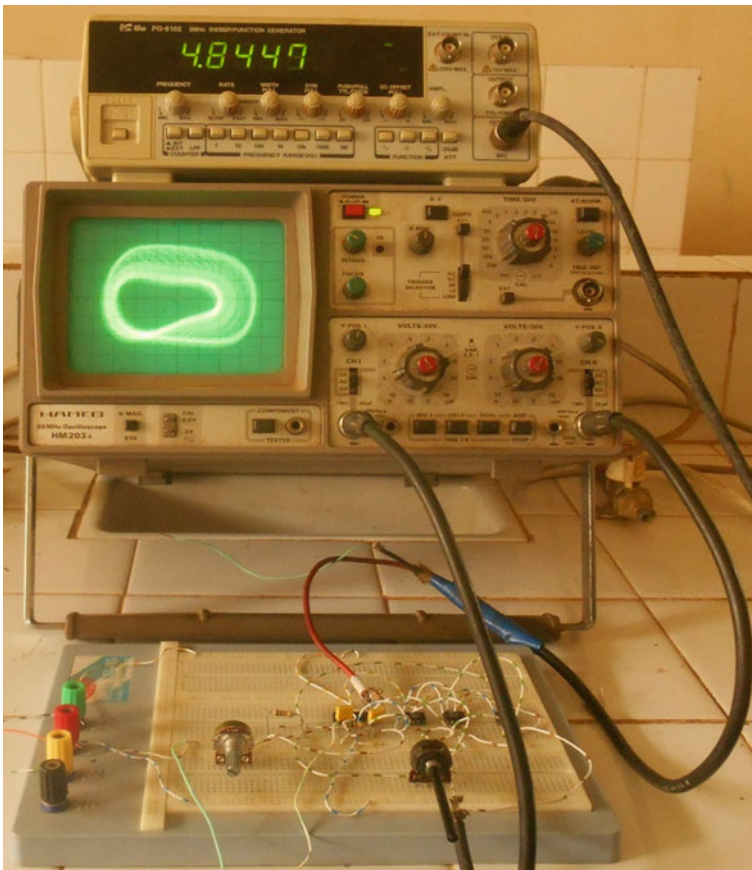


Fig. 4 Photograph of the analog oscilloscope displaying a single band chaotic attractor obtained from the electronic circuit of Fig. 3

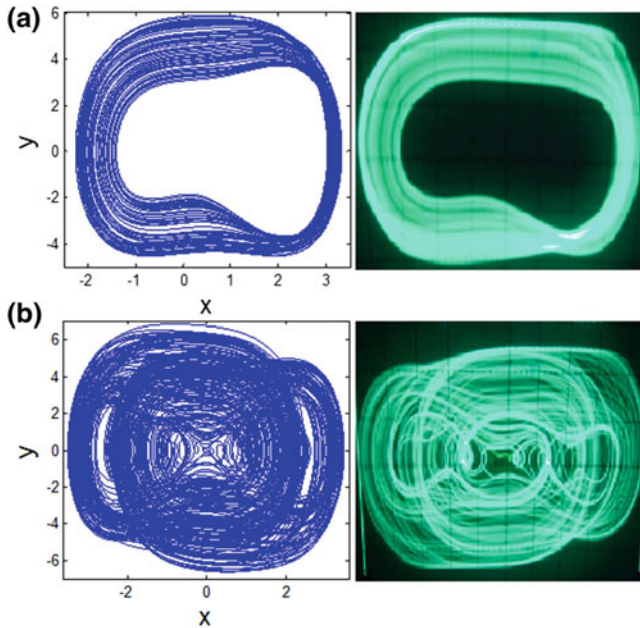


Fig. 5 Experimental phase portrait obtained from the Mathieu-Duffing oscillator using a dual-trace oscilloscope in XY mode. Corresponding numerical phase portraits are shown in the left. Output voltages V_x and V_y are fed to the X and Y input, respectively. **a** Single-band chaotic attractor for $R_4 = 1.92 \text{ k}\Omega$ and **b** double-band chaotic attractor for $R_4 = 1.72 \text{ k}\Omega$

A photograph of the analog oscilloscope displaying a single band chaotic attractor obtained from the electronic circuit of Fig. 3 is shown in Fig. 4.

The experimental results showing some dynamical behaviors of electronic circuit of Fig. 3 for some specific values of control parameter R_4 are shown in Fig. 5.

In light of the pictures in Fig. 5, one can note the good similarity of experimental portraits with those obtained numerically. This shows that the proposed electronic circuit is capable to reproduce the dynamics of the system under investigation. It should be stressed that system (2) can be also implemented using many other techniques such as integrated circuit technology (Trejo-Guerra et al. 2012), Field Programmable Analog Array (FPAA) technologies (Koyuncu et al. 2014) and Field

Programmable Gate Array (FPGA) (Fatma et al. 2016). The latter technology provides a fast prototype for investigating chaotic systems.

4 Adaptive Function Projective Synchronization of Two Identical Coupled Mathieu-Duffing Oscillators

In this section, we consider the problem of synchronization of Mathieu-Duffing oscillators with unknown parameters and external disturbances using adaptive function projective synchronization technique.

4.1 Problem Formulation

Let the drive and response systems be defined as

$$\dot{x} = F_1(t, x) + G_1(t, x)\varphi + D'(t) \quad (8)$$

$$\dot{y} = F_2(t, y) + G_2(t, y)\theta + D''(t) + u(t, x, y) \quad (9)$$

where $x, y \in R^n$, are the state variables of the drive and response systems, respectively, $F_1(t, x), F_2(t, y): R^n \rightarrow R^n$, $G_1(t, x) \in R^{n \times p}$, $G_2(t, y) \in R^{n \times q}$ are the continuous nonlinear functions, $\varphi \in R^p$, $\theta \in R^q$ are the unknown parameters of the drive and response system respectively, $D'(t) = [d_{11}, d_{12}, \dots, d_{1n}]^T \in R^n$ and $D''(t) = [d_{21}, d_{22}, \dots, d_{2n}]^T \in R^n$ represent the disturbance inputs with $|d_{1i}| \leq \lambda_i, (i = 1, 2, \dots, n)$ and $|d_{2i}| \leq \lambda_i, (i = 1, 2, \dots, n)$, and assume that $\lambda_i \geq 0$ are given, $\lambda_i = [\lambda_1, \lambda_2, \dots, \lambda_i]^T$ and $u(t, x, y)$ is the control function to be determined. Let us define the error state between the drive (8) and response (9) systems as follows

$$e(t) = x(t) - m(t)y(t) \quad (10)$$

where $m(t)$ is a continuously differentiable bounded function with $m(t) \neq 0$ for all t . The objective is to synchronize both drive and response systems to a scaling function $m(t)$ in presence of unknown parameters and external disturbances such that the error system (10) can be asymptotically stable at the zero equilibrium, i.e. $\|e(t)\| \rightarrow 0$ as $t \rightarrow \infty$.

Remark 1 If the scaling function $m(t)$ is a constant different from 1, the problem of function projective synchronization becomes projective synchronization. In the cases that $m(t) = 1$ and $m(t) = -1$, it turns out to be complete synchronization and antisynchronization, respectively (Chen and Li. 2007).

4.2 Main Results

Here, we suppose that the parameters in the drive system or response system are unknown. From Eq. (10), we can obtain the error dynamical system as

$$\dot{e}(t) = \dot{y}(t) - m(t)\dot{x}(t) - \dot{m}(t)x(t) \quad (11)$$

By substituting systems (8) and (9), we obtain

$$\begin{aligned} \dot{e}(t) = & F_2(t, y) + G_2(t, y)\theta - m(t)[F_1(t, x) + G_1(t, x)\varphi + D'(t)] \\ & - \dot{m}(t)x(t) + D''(t) + u(t, x, y) \end{aligned} \quad (12)$$

Theorem 1 *For the given scaling function $m(t)$, the adaptive FPS between drive system (8) and response system (9) can be achieved by the control function (13) and sufficient parameters update laws (14) and (15) as below*

$$\begin{aligned} u(t, x, y) = & m(t)[F_1(t, x) + G_1(t, x)\hat{\varphi}] - F_2(t, y) \\ & - G_2(t, y)\hat{\theta} + \dot{m}(t)x - ke - H(t, e)\rho \end{aligned} \quad (13)$$

$$\dot{\hat{\varphi}} = -G_1^T(t, x)m(t)e \quad (14)$$

$$\dot{\hat{\theta}} = G_2^T(t, y)e \quad (15)$$

where $H(t, e) = \tanh[m(t)(e_1, e_2, \dots, e_n)]$. In Eq. (15), $\hat{\varphi}$ and $\hat{\theta}$ are estimated values of unknown parameters φ and θ of the drive and the response system, respectively; $\tanh(\cdot)$ denotes the tangent hyperbolic function; $\rho = [\rho_1, \rho_2, \dots, \rho_n]^T$ is the boundaries of the uncertainties and $k = \text{diag}(k_1, k_2, \dots, k_n)$ is a gain matrix for each controller. The desired convergence rate can be adjusted by the gain matrix k .

Remark 2 In the control function (13), $H(t, e)\rho$ is a compensation term which is introduced to eliminate the influence of the disturbance inputs.

It is interesting to note that the conventional control methods often use the sign function (Hongyue et al. 2011; Fu 2012; Srivastava et al. 2013), but the discontinuity of the sign function causes the chattering and undesirable oscillations. In order to avoid these problems, in this chapter the discontinuous sign function is replaced by the continuous tangent hyperbolic function.

Proof Let $\tilde{\varphi} = \varphi - \hat{\varphi}$ and $\tilde{\theta} = \theta - \hat{\theta}$ be the parameter estimation errors. Choose the storage Lyapunov function of system (11) as

$$V = \frac{1}{2} \left(e^T e + \tilde{\varphi}^T \tilde{\varphi} + \tilde{\theta}^T \tilde{\theta} \right) \quad (16)$$

Thus, the time derivation of the Lyapunov function V along the trajectory of the error dynamics system (11) with following notations ($\dot{\tilde{\varphi}} = -\dot{\hat{\varphi}}$ and $\dot{\tilde{\theta}} = -\dot{\hat{\theta}}$) is

$$\begin{aligned} \dot{V} &= e^T \dot{e} + \tilde{\varphi}^T \dot{\tilde{\varphi}} + \tilde{\theta}^T \dot{\tilde{\theta}} \\ &= e^T [G_2(t, y)(\theta - \hat{\theta}) - m(t)G_1(t, x)(\varphi - \hat{\varphi}) - H(t, e)\rho] \\ &\quad + \tilde{\varphi}^T [G_1^T(t, x)m(t)e] + \theta^T [-G_2^T(t, y)e] - e^T ke - m(t)D'(t)e^T \\ &\quad + D''(t)e^T = -e^T ke - e^T H(t, e)\rho - m(t)D'(t)e^T + D''(t)e^T \end{aligned} \tag{17}$$

Let

$n_1 = e^T [D''(t) - m(t)D'(t)]$ and $n_2 = e^T H(t, e)\rho$ where $n_1, n_2 \in R$ and $n_2 \geq 0$. According to the definition and assumption of $D'(t), D''(t), \varphi$ and θ , it is guaranteed that $n_1 \leq n_2$, i.e. $n_1 - n_2 \leq 0$, then \dot{V} is written as

$$\dot{V} = -e^T ke + n_1 - n_2 \leq -e^T ke \leq 0 \tag{18}$$

Provided that \dot{V} is negative semi-definite, and since V is positive definite, it follows that $e \in L_\infty, \varphi, \theta \in L_\infty$. Thus $\dot{e} \in L_\infty$, and according to Eq. (11), it can be obtained that

$$\int_0^t \|e\|^2 dt = \int_0^t e^T e dt \leq -\frac{1}{l} \int_0^t \dot{V} dt = \frac{1}{l} [V(0) - V(t)] \leq \frac{1}{l} V(0) \tag{19}$$

Since $V(0) \leq \infty$ and $e \in L_2$, according to Barbalat's lemma, we have $\|e(t)\| \rightarrow 0$ as $t \rightarrow \infty$, i.e. the error dynamical system (11) will be stabilized at the zero equilibrium asymptotically. Thus, according to the Lyapunov stability theorem, the adaptive function projective synchronization between drive system (8) and response system (9) in presence of unknown parameters and external disturbances is achieved under the control function (13) and sufficient parameter update laws (14) and (15). However, we cannot conclude that the unknown parameters can be automatically estimated to their true values. The unknown parameters should be almost constant in some bounded interval (i.e. $\dot{\hat{\varphi}} = 0$ and $\dot{\hat{\theta}} = 0$). Another sufficient condition to guarantee the parameter identification based on the Linear Independence (LI) condition which is elaborated as follows. Using the Lasalle's Invariant Set Theorems (Zhiyong et al. 2012), the largest invariant set M can be obtained as

$$M = \{e \in R^n, \varphi \in R^p, \theta \in R^q | e = 0, G_2(t, y)\tilde{\theta} - m(t)G_1(t, x)\tilde{\varphi} - ke = 0\} \tag{20}$$

Thus one can get $G_2(t, y)\tilde{\theta} - m(t)G_1(t, x)\tilde{\varphi} = 0$. To ensure that this equation has the unique solution of $\tilde{\varphi} = 0$ and $\tilde{\theta} = 0$ (which implies that the unknown parameters

are estimated to their true values as $\hat{\varphi} = \varphi$, $\hat{\theta} = \theta$, the following condition (Linear Independence condition) should be satisfied. To achieve synchronization based on parameter identification of systems (8) and (9) with unknown parameters, the function elements in the function vector groups $-G_1^T(t, x)m(t)$ and $G_2^T(t, y)$ should be linearly independent on the synchronization manifold. Interested readers would consult (Yu et al. 2007) for more discussions. This completes the proof.

4.3 Application to Mathieu-Duffing Oscillator

For application we consider that the parameters of the drive system are known and those of the response system are unknown. With these considerations, the drive system is given as

$$\begin{cases} \dot{x}_1 = x_2 + d_1'(t) \\ \dot{x}_2 = -2\epsilon x_2 + \alpha x_1 - \gamma x_1^3 + \beta x_1 \sin(\omega t) + d_2'(t) \end{cases} \quad (21)$$

and the response system is given as

$$\begin{cases} \dot{y}_1 = y_2 + d_1''(t) + u_1(t, x, y) \\ \dot{y}_2 = -2\hat{\epsilon}y_2 + \hat{\alpha}y_1 - \hat{\gamma}y_1^3 + \hat{\beta}y_1 \sin(\omega t) + d_2''(t) + u_2(t, x, y) \end{cases} \quad (22)$$

Based on Theorem 1, the control functions and parameter update laws are determined by

$$u_1(t, x, y) = m(t)x_2 - y_2 + \dot{m}(t)x_1 - ke_1 - H(t, e_1) \quad (23a)$$

$$\begin{aligned} u_2(t, x, y) = m(t)[-2\epsilon x_2 + \alpha x_1 - \gamma x_1^3 + \beta x_1 \sin \omega t] + 2\hat{\epsilon}y_2 - \hat{\alpha}y_1 + \hat{\gamma}y_1^3 \\ - \hat{\beta}y_1 \sin \omega t + \dot{m}(t)x_2 - ke_2 - H(t, e_2) \end{aligned} \quad (23b)$$

and

$$\begin{cases} \dot{\hat{\epsilon}} = -y_2 e_2 \\ \dot{\hat{\alpha}} = y_1 e_2 \\ \dot{\hat{\gamma}} = -y_2^3 e_2 \\ \dot{\hat{\beta}} = y_1 \sin(\omega t) e_2 \end{cases} \quad (24)$$

In what follows, numerical simulations are given to verify the feasibility and the robustness of the proposed methods. The standard fourth-order Runge-Kutta method is applied to solve the differential equations describing the drive (21) and the response (22) systems with time step size equal to 0.005. The parameters values

of the drive system are selected as $\varepsilon = 0.125$, $\alpha = 1$, $\gamma = 1$, $\omega = 2$ and $\beta = 5.8$ so that it exhibits chaotic behaviors. The initial states are chosen as $x(0) = [0.1, 0.2]$ and $y(0) = [0.3, 0.4]$, respectively for the drive and response systems. The initial values of unknown parameters are set to be $\hat{\varepsilon}(0) = 0.006$, $\hat{\alpha}(0) = 0.015$, $\hat{\gamma}(0) = 0.07$ and $\hat{\beta}(0) = 0.08$. The control gains are set as $k_i = 20 (i = 1, 2)$. The scaling function is selected as $m(t) = 0.6 + 0.1 \sin(0.15\pi t)$. In order to verify the robustness of the method, we perform the numerical simulations in three cases (i) without external disturbances, (ii) with continuous time varying (sinusoidal type) and (iii) with white Gaussian noise. For the first case, the time response of the error system (11) and the synchronization quality which is defined by $e = \sqrt{e_1^2 + e_2^2}$ are shown in Fig. 6.

In Fig. 7, we show the time evolution of the parameter estimations in the response system.

Obviously, the synchronization errors converge to zero with exponentially asymptotical speed and two systems with different initial states achieve FPS very quickly. The unknown parameters of the response system are simultaneously successfully estimated to their true values.

For the second case, the external disturbances subjected to the drive and response systems are selected as $d'_1 = 0.1 \cos(0.2\pi t)$, $d'_2 = 0.2 \sin(0.3\pi t)$ and $d''_1 = 0.1 \sin(0.2\pi t)$, $d''_2 = 0.2 \cos(0.3\pi t)$. The boundaries of the uncertainties are chosen randomly as $\rho_1 = 0.8$ and $\rho_2 = 0.5$. The time response of the error system (11) and the synchronization quality are depicted in Fig. 8.

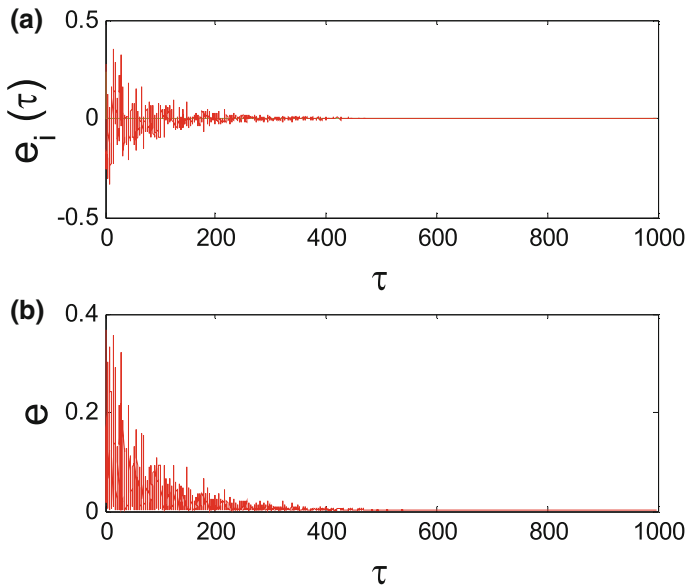


Fig. 6 Time dependence of the errors dynamics e_i ($i = 1, 2$) (a) and synchronization quality (b) between two coupled identical Mathieu-Duffing oscillators with FPS scheme without external disturbances

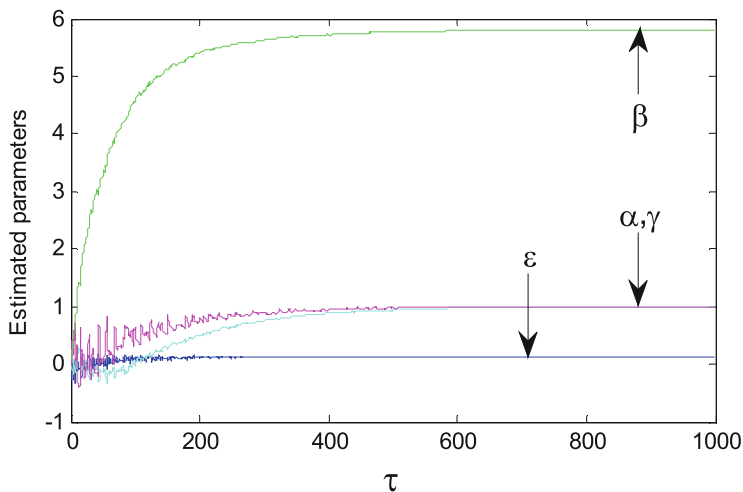


Fig. 7 Time evolution of the parameter estimations in the response system with FPS scheme without external disturbances

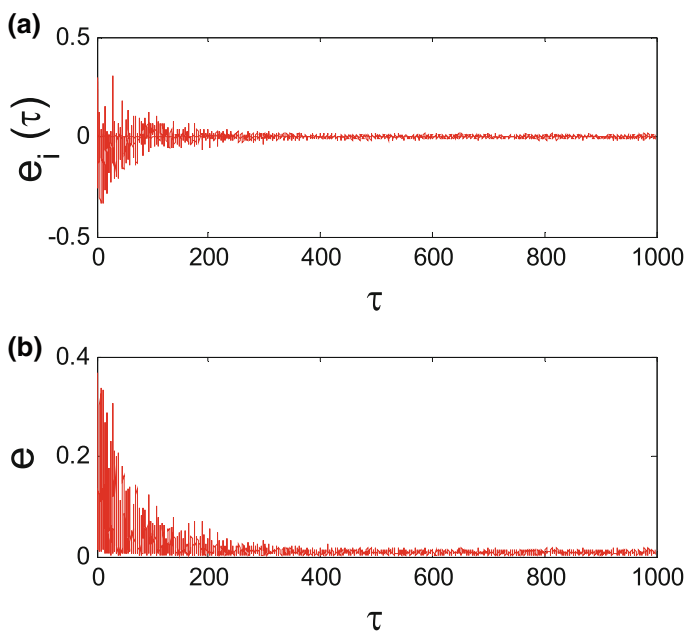


Fig. 8 Time dependence of the errors dynamics e_i ($i=1,2$) (a) and synchronization quality (b) between two coupled identical Mathieu-Duffing oscillators with FPS scheme with continuous time varying (sinusoidal type) external disturbances

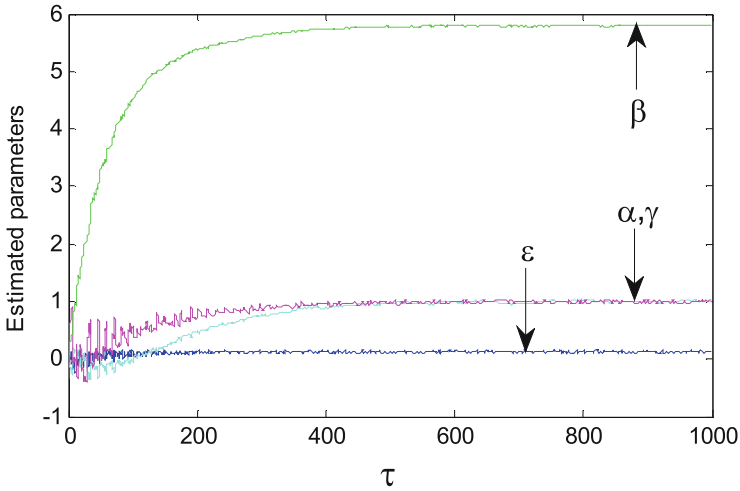


Fig. 9 Time evolution of the parameter estimations in the response system with FPS scheme with continuous time varying (sinusoidal type) external disturbances

The time evolution of the parameter estimations in the response system subjected to a continuous time varying (sinusoidal type) external disturbances are depicted in Fig. 9.

As can be seen from those figures, the synchronization errors and synchronization quality arrive at zero in finite time and the unknown parameters in the

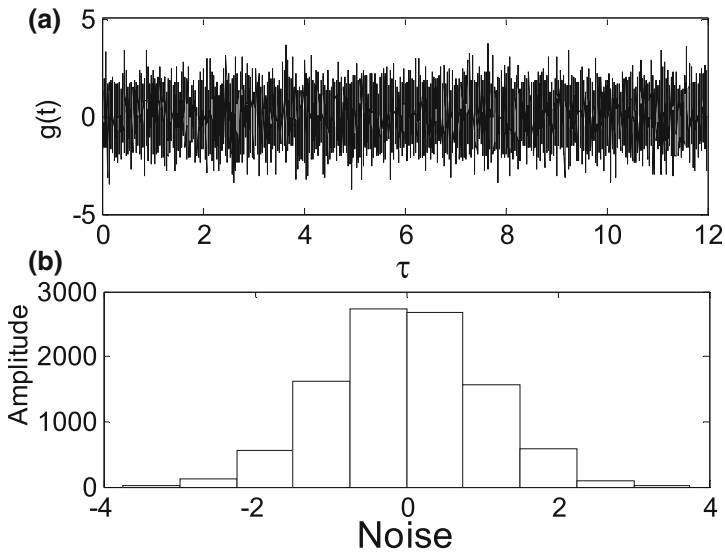


Fig. 10 Time evolution of a white Gaussian noise (a) and its histogram in the range $[-4, 4]$ (b)

response system have been estimated to their true values in spite of the presence of the external disturbances. The effect of the external disturbances is clearly visible on the errors dynamics as well as on the estimation of the unknown parameters.

In the last case, external disturbances subjected to drive and response systems are the white Gaussian noises chosen as $d'_1 = d'_2 = \sqrt{(-2 \ln \lambda)} \sin(2\pi\lambda)$ and $d_2 = d_1 = \sqrt{(-2 \ln \lambda)} \cos(2\pi\lambda)$ where λ is the random function. The control gains are set as $k_i = 10$ ($i = 1, 2$). In Fig. 10, we show the white Gaussian noise and its histogram in the range $[-4, 4]$.

The time response of the error system (11) and the synchronization quality are displayed in Fig. 11.

The time evolution of the parameter estimations in the response system subjected to a white Gaussian noise are depicted in Fig. 12.

One can see from those figures that the synchronization errors and synchronization quality converge to zero and the unknown parameters in the response system have been estimated approximatively to their true values. The effect of the external disturbances is more visible on the errors dynamics as well as on the estimation of the unknown parameters. All these results demonstrate that the FPS in the coupled identical Mathieu-Duffing oscillators via control functions (23) and

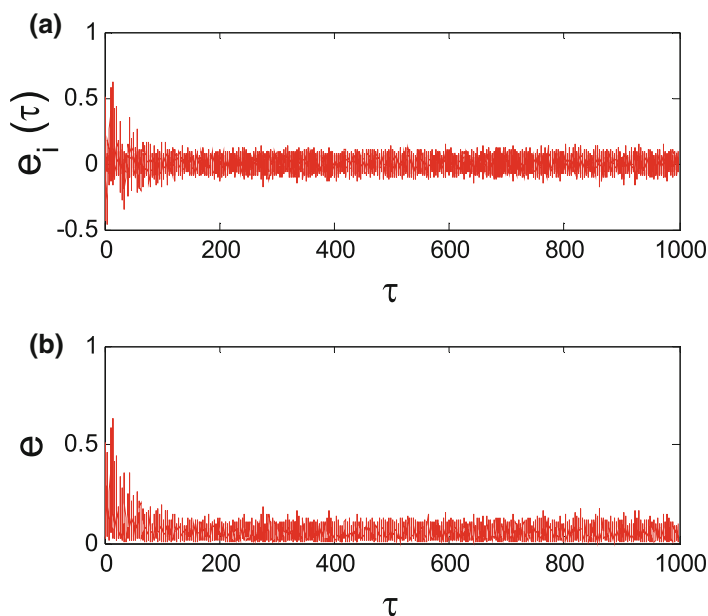


Fig. 11 Time dependence of the errors dynamics e_i ($i = 1, 2$) (a) and synchronization quality (b) between two coupled identical Mathieu-Duffing oscillators with FPS scheme with white Gaussian external noise

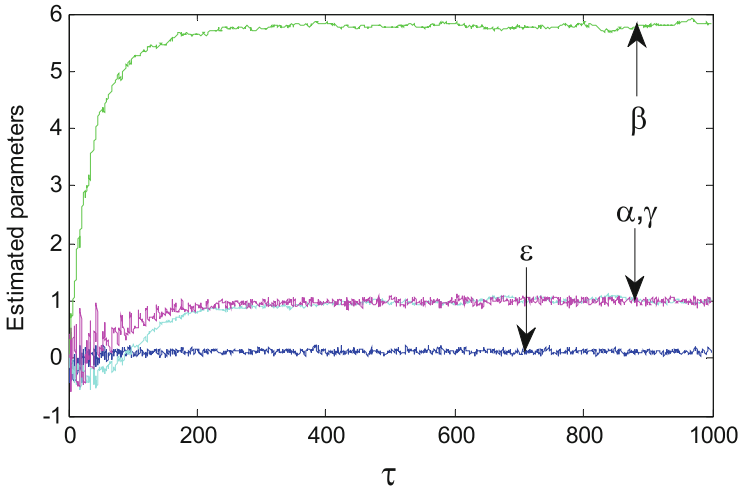


Fig. 12 Time evolution of the parameter estimations in the response system with FPS scheme with white Gaussian external noise

parameter update laws (24) is obtained with estimation of the unknown parameters of the response system and in presence of external uncertainties at the desired scaling function $m(t)$.

5 Concluding Remarks

The dynamics of a Mathieu-Duffing oscillator has been investigated numerically and experimentally in this chapter. The dynamical properties of the oscillator have been examined using classical nonlinear analysis techniques such as bifurcation diagram, plot of largest Lyapunov exponent and frequency spectrum. It was found from the bifurcation structure that the system experiences very rich and complex behaviors including periodicity, quasi-periodicity and chaos. An experimental study has been carried out and the laboratory experimental measurements were in a good qualitative agreement with numerical results. Furthermore, using the Lyapunov stability theory, we have designed adaptive controllers and sufficient parameter update laws able to achieve the function projective synchronization between two identical drive-response structures of Mathieu-duffing oscillators with unknown parameters. We have introduced the external disturbances in the drive and response systems in order to verify the robustness of our proposed strategy. It has been noted that the unpredictable properties of the scaling function $m(t)$ can additionally enhance the security of the communication. Theoretical results and numerical simulations were finally included to visualize the effectiveness and feasibility of the developed methods. We stress also that the approach followed in this chapter may

be exploited rigorously to the study of any other nonlinear dynamical system driven by an external force.

Acknowledgements V. Kamdoun Tamba wishes to thank Dr. Sifeu Takougang Kingni (University of Maroua, Cameroon) for interesting discussions and careful reading of the chapter.

References

- An H-L, Chen Y (2009) The function cascade synchronization scheme for discrete-time hyperchaotic systems. *Commun Nonlinear Sci Numer Simul* 14:1494–1501
- Banerjee R (2010) *Chaos Synchronization and Cryptography for Secure communications*. IGI Global, USA
- Buscarino A, Fortuna L, Frasca M (2009) Experimental robust synchronization of hyperchaotic circuits. *Phys D* 238:1917–1922
- Chen Y, Li X (2007) Function projective synchronization between two identical chaotic systems. *Int J Mod Phys C* 18:2246–2255
- Chitra RN, Kuriakose VC (2008) Phase synchronization in an array of driven Josephson junctions. *Chaos* 18:0131251
- Corless RM, Parkinson GV (1988) A model of the combined effects of vortex-induced vibration and galloping. *J Fluids Struct* 2:203–220
- Corless RM, Parkinson GV (1993) A model of the combined effects of vortex-induced vibration and galloping part II. *J Fluids Struct* 7:825–848
- Dalkiran Fatma Yildirim, Sprott JC (2016) Simple chaotic hyperjerk system. *Int J Bifurcat Chaos* 26:1650189
- Fei Y, Chunhua W, Qiuzhen W, Yan H (2013) Complete switched modified function projective synchronization of a five-term chaotic system with uncertain parameters and disturbances. *Pramana J Phys* 80:223–235
- Fu G (2012) Robust adaptive modified function projective synchronization of hyperchaotic systems subject to external disturbance. *Commun Nonlinear Sci Numer Simul* 17:2602–2608
- Guckenheimer J, Holmes PJ (1984) *Nonlinear oscillations, dynamical systems, and bifurcations of vector fields*. Springer, Berlin
- Hayashi C (1964) *Nonlinear oscillations in physical systems*. McGraw Hill, New York
- Hongyue D, Feng L, Guangshi M (2011) Robust function projective synchronization of two different chaotic systems with unknown parameters. *J Franklin Inst* 348:2782–2794
- Kareem SO, Ojo KS, Njah AN (2012) Function projective synchronization of identical and non-identical modified finance and Shimizu-Morioka systems. *Pramana J Phys* 79:71–79
- Koyuncu I, Ozecerit AT, Pehlivan I (2014) Implementation of FPGA-based real time novel chaotic oscillator. *Nonlinear Dyn* 77:49–59
- Li X, Chen Y (2007) Function projective synchronization of two identical new hyperchaotic systems. *Commun Theoret Phys* 48:864–870
- Ma J, Wu X, Chu R et al (2014) Selection of multi-scroll attractors in Jerk circuits and their verification using Pspice. *Nonlinear Dyn* 76:1951–1962
- Mahmoud GM, Mansour EA (2011) A hyperchaotic complex system generating two-, three-, and four-scroll attractors. *J Vib Control* 18:841–849
- Moon FC, Johnson MA (1998) *Nonlinear dynamics and chaos in manufacturing processes*. Wiley, New York
- Parlitz U, Lauterborn W (1987) Period-doubling cascades and devil's staircases of the driven van der Pol oscillator. *Phys Rev A* 36:1428–1434
- Pecora LM, Carroll TL (1990) Synchronization in chaotic systems. *Phys Rev Lett* 64:821–824

- Ping Z, Yu-xia C (2010) Function projective synchronization between fractional-order chaotic systems and integer-order chaotic systems. *Chin Phys* 19:100507–100511
- Press WH, Teukolsky SA, Vetterling WT, Flannery BP (1992) Numerical recipes in Fortran, vol 77. Cambridge University Press
- Rajasekar S, Parthasarathy S, Lakshmanan M (1992) Prediction of horseshoe chaos in BVP and DVP oscillators. *Chaos, Solitons Fractals* 2:208–271
- Sharma Anjali, Patidar Vinod, Purohit G, Sud KK (2012) Effects on the bifurcation and chaos in forced Duffing oscillator due to nonlinear damping. *Commun Nonlinear Sci Numer Simul* 17:2254–2269
- Shen J, Chen S (2009) An open-plus-closed-loop control for chaotic Mathieu-Duffing oscillator. *Appl Math Mech Engl Ed* 30:19–27
- Shen JH, Lin KC, Chen SH, Sze KY (2008) Bifurcation and route-to-chaos analyses for Mathieu-Duffing oscillator by the incremental harmonic balance method. *Nonlinear Dyn* 52:403–414
- Siewe Siewe M, Tchawoua C, Wofo P (2010) Melnikov chaos in a periodically driven Rayleigh-Duffing oscillator. *Mech Res Commun* 37:363–368
- Srivastava M, Agrawal SK, Subir D (2013) Adaptive projective synchronization between different chaotic systems with parametric uncertainties and external disturbances. *Pramana J Phys* 81:417–437
- Steeb WH, Kunick A (1987) Chaos in limit cycle systems with external periodic excitation. *Int J Nonlinear Mech* 1987(349):361–422
- Tejo-Guerra R, Tlelo-Cuautle E, Jimenez-Fuentes JM, Sanchez-Lopez C, Munoz-Pacheco JM, Espinosa-Flores-Verdad G, Rocha-Perez JM (2012) Integrated circuit generating 3- and 5-scroll attractors. *Commun Nonlinear Sci Numer Simul* 17:4328–4335
- Venkatesan A, Lakshmanan M (1997) Bifurcation and chaos in the double-well Duffing-van der Pol oscillator: numerical and analytical studies. *Phys Rev E* 56:6321–6330
- Vincent UE, Laoye JA, Kareem SO (2008) Control and synchronization of chaos in RCL-shunted Josephson junction using backstepping design. *Physica C* 468:374–382
- Volos CK, Kyprianidis IM, Stouboulus INA (2012) Chaotic path planning generator for autonomous mobile robots. *Robot Auton Syst* 60:651–656
- Volos CK, Kyprianidis IM, Stouboulus IN (2013a) Image encryption process based on chaotic synchronization phenomena. *Signal Process* 93:1328–1340
- Volos CK, Kyprianidis IM, Stouboulus IN (2013b) Experimental investigation on coverage performance of a chaotic autonomous mobile robot. *Robot Auton Syst* 61:1314–1322
- Wen SF, Shen YJ, Wang XN, Yang SP, Xing HJ (2016) Dynamical analysis of strongly nonlinear fractional-order Mathieu-Duffing equation. *Chaos* 26:084309
- Wen SF, Shen YJ, Yang SP, Wang J (2017) Dynamical response of Mathieu-Duffing oscillator with fractional-order delayed feedback. *Chaos, Solitons Fractals* 94:54–62
- Wolf A, Swift JB, Swinney HL, Wastano JA (1985) Determining Lyapunov exponents from time series. *Phys D* 16:285–317
- Yang M, Cai B, Cai G (2010) Projective synchronization of a modified three dimensional chaotic finance system. *Int J Nonlinear Sci* 10:32–38
- Yang JH, Sanjuan MAF, Liu HG (2015) Bifurcation and resonance in a fractional Mathieu-Duffing oscillator. *Eur Phys J B* 88:310–318
- Yu P, Shah AH, Popplewell N (1992) Inertially coupled galloping of iced conductors. *ASME J Appl Mach* 59:140–145
- Yu P, Desai YM, Shah AH, Popplewell N (1993a) Three-degree-of-freedom model for galloping. Part I Formulation *ASME J Eng Mech* 119:2404–2425
- Yu P, Desai YM, Popplewell N, Shah AH (1993b) Three-degree-of-freedom model for galloping. Part II Solutions *ASME J Eng Mech* 119:2426–2448
- Yu W, Chen G, Cao J, Lu J, Parlitz U (2007). Parameter identification of dynamical systems from time series, *Phys. Rev. E*, 75: 067201–067204

- Zhan M, Wang X, Gong X, Wei GW, Lai CH (2003) Complete synchronization and generalized synchronization of one-way coupled time-delay systems. *Phys Rev E Stat Nonlinear Soft Matter Phys* 68:036208
- Zhiyong S, Gangauan S, Fuhong M, Yanbin Z (2012) Adaptive modified function projective synchronization and parameter identification of uncertain hyperchaotic (chaotic) systems with identical or non-identical structures. *Nonlinear Dyn* 68:471–486
- Zhu S, Wu L (2004) Anticipating and lag synchronization in chaotic laser system. *Int. J. Mod. Phys. B* 18:2547–2551
- Zhu HL, Zhang XB (2009) Modified Projective Synchronization of different hyperchaotic systems. *J Inf Comput Sci* 4:33–40